Astronomy & Astrophysics manuscript no. output
April 30, 2021

On the stability of the ICRF axes

N. Liu[1,2], S. B. Lambert[3], J.-C. Liu[1], and Z. Zhu[1]

[1] School of Astronomy and Space Science, Key Laboratory of Modern Astronomy and Astrophysics (Ministry of Education), Nanjing University, Nanjing 210023, P. R. China
e-mail: [niu.liu;jcliu;zhuzi]@nju.edu.cn
[2] School of Earth Sciences and Engineering, Nanjing University, Nanjing 210023, P. R. China
[3] SYRTE, Observatoire de Paris, Université PSL, CNRS, Sorbonne Université, LNE, Paris, France
e-mail: sebastien.lambert@obspm.fr

Received; accepted

ABSTRACT

Context.
Aims.
Methods.
Results.
Conclusions.

Key words. reference systems – astrometry – techniques: interferometric – quasars: general – catalogs

1. Introduction

The celestial reference frame (CRF) provides the basic position reference widely used in the astronomy and geoscience. The current realization of the CRF as adopted by the International Astronomical Union (IAU) in 2018 is the third realization of the International Celestial Reference Frame (ICRF3; Charlot et al. 2020). The ICRF3 is materialized by positions of more than 4000 extragalactic sources based on very long baseline interferometry (VLBI) observations made at the dual S/X-, K-, and X/Ka-band since 1979. With several improvements in the modelling, for example, the correction of the Galactic aberration effect due to the acceleration of the solar system barycenter (MacMillan et al. 2019), and more accumulated data, the best position precision achieved for individual sources in the ICRF3 has reach a level of 30 micro-arcsecond (μas).

The extragalatic sources are used to construct the ICRF because they are distant from us so that they appear more compact than other objects like Galatic stars with a stable position in the sky. However, the apparent position of the extragalatic source varies with time, both in the radio and optical domain (e.g., see Andrei et al. 2009; Lambert 2013). This kind of position variability of extragalatic sources, sometimes also referred to as the astrometric stability, would lead to variations in the direction of the celestial frame axes defined by positions of those sources. This phenomenon is known as the celestial frame instability (e.g., Lambert et al. 2008), a common issue for all kinds of extragalatic celestial reference frame such as the ICRF and the *Gaia* celestial frame (*Gaia*-CRF; Gaia Collaboration et al. 2018). This celestial frame instability would introduce additional noises to the VLBI products such as the Earth orientation parameters (EOP); the implication would be more serious for the nutation series since so far the VLBI is the sole technique that can determine the nutation angle. Dehant et al. (2003); Lambert et al. (2008) study the impact of the celestial frame instability on the estimate of the nutation terms from the VLBI observations and report an additional noise of 15 μas in the amplitude of 18.6-year nutation term. The variability of extragalatic source might also degrade the precision of VLBI-*Gaia* frame link (Taris et al. 2013, 2016, 2018). Therefore, it is necessary to assess and monitor the instability level of the celestial reference system. This work focuses on the axis stability of the ICRF materialized by VLBI observations.

There are several possibilities that make radio source apparent position unstable. The main origin is the temporal evolution of radio source structure due to intrinsic variability such as the ejection of new jet features, which could manifest itself as an apparent proper motion (linear drift) of radio sources (Fomalont et al. 2011; Moór et al. 2011). Other causes include the difference of radio source position as "seen" by different VLBI network (Dehant et al. 2003) and the weak micro-lensing effect (Sazhin et al. 1998).

Several authors have proposed indicators to characterize the radio source position stability. Statistics based on the source coordinate time series are often used, e.g., slope and standard deviation (Feissel-Vernier 2003), Allan variance (Gattano et al. 2018). The ICRF Working Group uses a quantity considering the coordinate variations (weighted root-mean-square, WRMS) and the reduced chi-square for right ascension and declination (Fey et al. 2015; Charlot et al. 2020). In addition, other authors construct indicators based on the interstellar scintillation around the source (Schaap et al. 2013) and flux density time series (light curve; Shabala et al. 2014), which are found to be correlated with the position stability. Based on these indicators, sources with an unstable positions can be recognized and ruled out, leaving these stable sources to define and maintain the axes of the ICRF, which is known as the so-called defining source (Feissel-Vernier 2003; Feissel-Vernier et al. 2006; Lambert & Gontier 2009). The stability of the VLBI celestial reference frame can be thus improved when a proper ensemble of stable sources are used as the defining source (Arias & Bouquillon 2004; Liu et al. 2017).

Table 1. Statistics of number of sources in catalogs used in this work.

Catalog	All	Com. to ICRF3 S/X	ICRF3 Def.
ICRF2	3414	3410	296
ICRF3 K	793	550	193
ICRF3 X/Ka	638	450	176
asi2020a	4447	4296	290
aus2020b	4817	4456	299
opa2019a	4468	4380	303
usn2019c	2390	2263	292

The ICRF axes are found to be stable on a level of 20 μas (Ma et al. 1998), which is further improved to 10 μas for the ICRF2 (Fey et al. 2015). These results are based on comparing the relative orientation of various subsets of sources. Adopting a different method, Lambert (2013) constructs the yearly celestial reference frame from the radio source coordinate time series. The author finds that the axis stability of the ICRF2 does not degrade after 2009, which is around 20 μas for each axis. Later, Lambert (2014) compares VLBI radio source catalogs submitted from different analysis centers of the International VLBI Service for Geodesy and Astrometry (IVS; Nothnagel et al. 2017) and reports an agreement of several tens of μas among these catalogs. Recently, Gattano et al. (2018) study the astrometric stability of extragalactic sources in the light of the Allan standard deviation of VLBI position time series. They conclude that the source position showing a stable behavior is likely to become unstable within a longer time span. It highlights the need of regularly monitoring the astrometric behaviors of radio sources and the axis stability of the ICRF, as already pointed out in Lambert (2013).

This work aims to re-assess the stability of ICRF axes. To achieve this goal, we adopted different methods used in the literature as well as developed our own method (Sect. 3) and compared the results (Sect. 4). Considering that the ICRF3 is materialized in three frequencies and that the *Gaia* catalog also provide an optical realization of the ICRF, we evaluated the agreement of the axis direction of these catalogs (Sect. 4.4). This analysis serves as a check of the consistency of ICRF axes at different frequencies and also a preview of the potential precision of the VLBI-*Gaia* frame link.

2. Data

2.1. Catalogs

The ICRF3 catalog (Charlot et al. 2020) was retrieved from the Paris Observatory IERS ICRS center. [1] We took the AGN sample (`gaiaedr3.agn_cross_id` table) in the *Gaia* EDR3 from the *Gaia* archive[2], where we found optical counterparts for 3181 ICRF3 sources via the external catalog name (column "`catalogue_name`") for identifying these sources. There are 3142 sources in the *Gaia* EDR3 common to the ICRF3 S/X-band catalog, 660 common to the K-band catalog, and 576 for the X/Ka-band.

[1] https://hpiers.obspm.fr/icrs-pc/newwww/icrf/index.php

[2] http://gea.esac.esa.int/archive/

We used four radio source catalogs which are publicly available at the IVS data center.[3] These solutions were: asi2020a from the the Space Geodesy Centre of the Italian Space Agency, aus2020b from the Geoscience Australia, opa2019a from the Paris Observatory, France, and usn2019c from the Unites States Naval Observatory. The solution aus2020b was obtained with the OCCAM geodetic VLBI analysis software package (Titov et al. 2004), while the rest catalogs were obtained from the Calc/Solve package developed and maintained by the VLBI group at NASA/GSFC (Ma et al. 1986). Sources whose position was estimated with no more than three observables were removed from the list; this was done for all four catalogs.

Table 1 tabulates statistics of number of sources in these catalogs mentioned above, as well as the subset of sources common among them.

2.2. VLBI observations and global solutions

We used the dual S/X-band VLBI observations made during 1979-2021, in total 6864 regular sessions and nearly 15 million observables (group delays). [4] These data were reprocessed by the Calc/Solve in the global solution mode, following an identical configuration and parameterization to the solution opa2019a. The detailed technique description can be found at the Paris Observatory Geodetic VLBI Center. [5] In the resulting radio source catalogs, sources whose position was estimated with less than three group delays were also removed.

2.3. Radio source coordinate time series

We used the radio source coordinate time series available at Paris Observatory Geodetic VLBI Center.[6] These time series are derived from the geodetic/astrometric VLBI observations starting from 1979 and will be periodically updated. The parameterization and a priori model choice of the VLBI solutions were almost identical to those used for deriving the opa2019a solutions, except some special configurations of radio source position and celestial frame maintenance; for later we referred to Lambert (2013) for a detailed description. We downloaded the coordinate time series for 4879 radio sources on on March 15, 2021, which were derived based the VLBI observations spanning from 1979.6 to 2021.2. There are 4538 sources in common with the ICRF3 catalogs, including all the 303 ICRF3 defining sources.

3. Methods

The axis stability of the celestial frames were evaluated by three methods:

1. We estimated the apparent proper motions (slope) from coordinate time series of extragalactic sources and then fitted the global spin vector based on these apparent proper motions. The spin multiplied by the time span gives an estimate of the axis stability.

[3] These catalogs are available via anonymous ftp to ftp://ivsopar.obspm.fr/vlbi/ivsproducts/crf

[4] A regular session is a collection of VLBI observations made within 24 hours (a day). The full session list can be found at http://ivsopar.obspm.fr/24h/opa2019a.arc, whereas sessions after January 1st, 2021 therein were used in this work.

[5] http://ivsopar.obspm.fr/24h/opa2019a.eops.txt

[6] http://ivsopar.obspm.fr/radiosources/index.php

2. We constructed the yearly celestial reference frame from the coordinate time series and VLBI global solutions of observations with different time span, respectively, and compared the relative orientation of these yearly CRFs with referred to the ICRF3 S/X-band catalog. The dispersion of the relative orientation angles provides a metrics of the stable stability.
3. We compared various representations of the ICRF from VLBI global solutions with different analysis strategies and fitted the relative orientation of these representations with referred to the ICRF3 based on the subset of the ICRF3 defining sources.

3.1. Modelling of the global difference

The global (large-scale) features in any vector filed on the celestial sphere can be described by the vector spherical harmonics (VSH). Here we only considered the first degree of the VSH, which consists of a rotation vector $\boldsymbol{R}$ and a glide vector $\boldsymbol{G}$. The full equation can be expressed as

$$\begin{aligned}\Delta_{\alpha^*} = &\ -R_1\cos\alpha\sin\delta - R_2\sin\alpha\sin\delta + R_3\cos\delta \\ &\ -G_1\sin\alpha + G_2\cos\alpha, \\ \Delta_\delta = &\ +R_1\sin\alpha - R_2\cos\alpha \\ &\ -G_1\cos\alpha\sin\delta - G_2\sin\alpha\sin\delta + G_3\cos\delta,\end{aligned} \tag{1}$$

where $\boldsymbol{R} = (R_1, R_2, R_3)^{\mathrm{T}}$ and $\boldsymbol{G} = (G_1, G_2, G_3)^{\mathrm{T}}$. The rotation vector consists of the rotations around the X-, Y-, and Z-axis and was used to characterize the stability of the ICRF axes.

Since we dealt with the rotation vectors both from the position offset and apparent proper motion vector field, different notations were used for clarity. Following the conventions used, e.g., in Gaia Collaboration et al. (2018), we used the term "orientation" to represent the rotation vector estimated from the position offset and "spin" for that from the proper motion data, which means that $(\Delta_{\alpha^*}, \Delta_\delta)$ in Eq. (1) were substituted by $(\Delta\alpha^*, \Delta\delta)$ and $(\mu_{\alpha^*}, \mu_\delta)$. The orientation vector, referred to as $\boldsymbol{\epsilon} = (\epsilon_x, \epsilon_y, \epsilon_z)^{\mathrm{T}}$, contain three orientation angles of the X-, Y-, and Z-axis among catalogs and can be used to align the catalogs. The spin vector $\boldsymbol{\omega} = (\omega_x, \omega_y, \omega_z)^{\mathrm{T}}$ models the change rate of the ICRF axis direction due to the (apparent) proper motion of extragalatic sources.

The rotation signal was estimated through the least-square (LSQ) fitting to the position offset and proper motion weighted by their formal uncertainties. We used an similar algorithm as that in Liu et al. (2020) to remove outliers. The rotation and glide vectors are orthogonal to each other, so that the existence of glide (rotation) signal should not affect the estimate of the rotation (glide) parameters for an ensemble of sources uniformly distributing on the sphere. However, this condition can never be fulfilled in the real world. In this work, the glide parameters were estimated together with the rotation terms in the LSQ fitting in order to reduce possible bias in the estimate of rotation parameters leaked from the glide signal, but will not be discussed or presented. We compared the fitted results of the rotation vector with and without including the glide vector in the transformation model and found consistent results within the formal uncertainties.

3.2. Global rotation signal from bootstrap sampling

In this work, we mainly estimated the rotation signal using the subset consisted of the ICRF3 defining sources. In addition, in order to avoid possible bias when considering exclusively one subset, e.g., unreliable apparent proper motion of some sources, we considered the whole sample and a robust estimate of the global rotation signal was obtained by the bootstrap sampling. That is, we picked randomly N sources from the sample (without replacement) and estimated the rotation parameters. This procedure was repeated 1000 times and we calculated the mean and standard deviation of the rotation parameters as the estimate value and associated formal uncertainty. This method was adopted to estimate the relative orientations between catalogs.

3.3. Apparent proper motion of radio sources

We estimated the apparent proper motion (linear drift) of the radio source based on their time series through a weighted LSQ fitting. This model can be described as following:

$$\alpha\cos\delta = \mu_{\alpha*}(t - t_0) + \alpha_0\cos\delta,\ \ \delta = \mu_\delta(t - t_0) + \delta_0, \tag{2}$$

where $\mu_{\alpha*}$ and μ_δ are apparent proper motions in the right ascension (R.A.) and declination (decl.), respectively, t_0 the mean epoch of the observing span for a given source. The notation $\alpha* = \alpha\cos\delta$ will be used throughout this work. All the data points were weighted by the inverse of the square of their formal uncertainties. Besides, the correlation between the R.A. and decl. were considered in the LSQ fitting, which means that $\mu_{\alpha*}$ and μ_δ were fitted simultaneously. These data points whose distance to their mean value is greater than three times of their formal uncertainties were removed before estimating $\mu_{\alpha*}$ and μ_δ to prevent the possible bias caused by these unreliable measurements. Sources with less than five data points in the remaining time series for either R.A. or decl. were also removed from our list. In the end, we obtained the apparent proper motion measurements for 1006 sources, 290 included in the ICRF3 defining source list.

3.4. Construction of yearly celestial reference frame

Two approaches were used to construct the yearly celestial refe rence frames. On the one hand, we truncated the VLBI observations, starting from 1979, at a certain year which ranges from 1985 to 2021 with a step of one year and used these observations as the input of the VLBI global solution. Earlier years were not considered due to the scarcity of observations. Thus, we ran 37 separated VLBI global solutions. On the other hand, we averaged the source position from the coordinate time series within an one-year moving window with a step of also one-year, i.e., without overlaps, since 1985. By doing, we formed another version of 36 yearly celestial frames.

4. Results

4.1. Global spin from apparent proper motion

We obtained the apparent proper motion for 1006 sources, 290 sources being classified as the so-called ICRF3 defining source. The median value of the apparent proper motion for all sources is 0.7 μas yr^{-1} in the R.A. and 1.6 μas yr^{-1} in the decl., respectively; they are 1.1 μas yr^{-1} and $-3.0\,\mu$as yr^{-1} for the ICRF3 defining source subset. For most sources ($\gtrsim$70%) in the sample, the apparent proper motion is within $\pm\,25\,\mu$as yr^{-1} either in the R.A. or the declination.

We fitted the global spin from the apparent proper motion. We first considered the 290 sources among the ICRF3 defining source list, and the reported the result below.

$$\begin{aligned}\omega_x &= -0.65 \pm 0.41\,\mu\mathrm{as\,yr^{-1}}, \\ \omega_y &= +0.26 \pm 0.41\,\mu\mathrm{as\,yr^{-1}}, \\ \omega_z &= +0.80 \pm 0.28\,\mu\mathrm{as\,yr^{-1}}.\end{aligned} \tag{3}$$

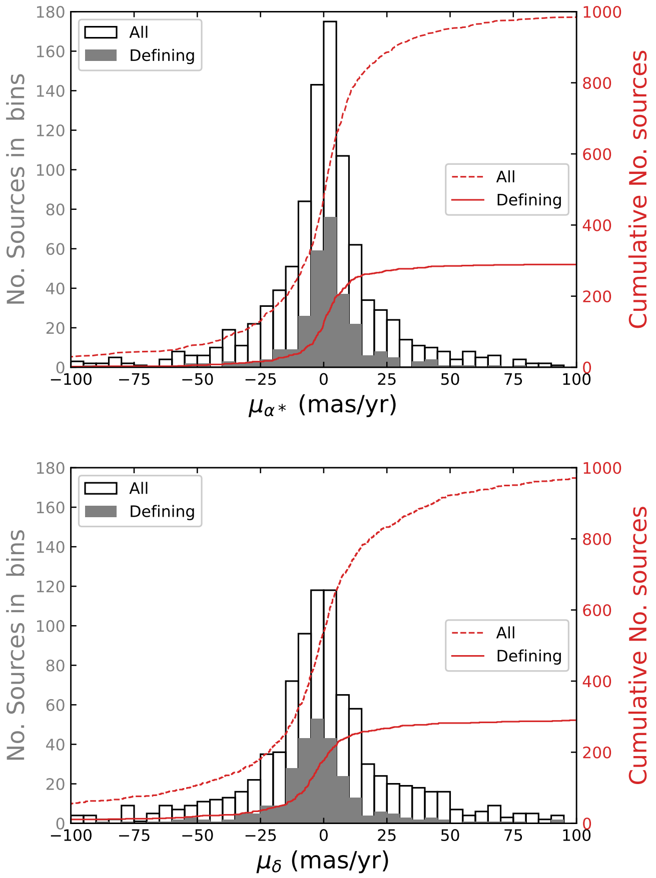

Fig. 1. Distribution of the apparent proper motion in the right ascension (*left*) and declination (*right*) for 1006 radio sources fitted from their coordinate time series. The left and right vertical axes indicates the number of sources in the each bin and cumulative from the leftmost bin. The distribution for 290 sources among the so-called 303 ICRF3 defining source list were labelled in different markers.

We then estimated the global spin from the whole sample using the bootstrap sampling as described in Sect. 3.2. The sample size N varies from 100 to 1000, with a step of 100. Figure. 4.1 presents the distribution of the mean spin (marker) and the standard deviation (errorbar) as a functions of N. We found that the spin parameters were generally stable around some certain values, i.e., $\omega_{\rm x} \sim -0.7\,\mu{\rm as\,yr^{-1}}$, $\omega_{\rm y} \sim -0.1\,\mu{\rm as\,yr^{-1}}$, and $\omega_{\rm z} \sim +0.6\,\mu{\rm as\,yr^{-1}}$.

By taking the global spin value of $\sim 0.8\,\mu{\rm as\,yr^{-1}}$ and considering the time span of 41.6 yr long (1979.6-2021.2), the accumulated deformation (orientation angle) in either axis of the VLBI celestial reference frame is about 33 μas. This gives a rather conservation estimate of the ICRF axis stability since the global spin could be indeed smaller, for example, consistent with zero spin for the Y-axis when considering the formal uncertainty.

4.2. Orientation of yearly CRFs relative to the ICRF3

Figure 3 depicts the orientation of the yearly celestial reference frames from the VLBI solutions with respect to the ICRF3 S/X-band catalog. The dispersion of the orientation angle reduces significantly after 1995, especially after 2015 which is the reference epoch of the ICRF3 catalog, except an abrupt change at 2002 and 2003 (*WHY?*). The weighted mean value of the orientation angle is +26 μas, −41 μas, and −4 μas for the X-, Y-, and Z-axis, respectively. The corresponding standard deviations are 22 μas, 24 μas, and 22 μas. If removing these data points before 1995 and at 2002-2003, the mean values change little whereas the standard deviations were reduced to 16 μas, 19 μas, and 16 μas.

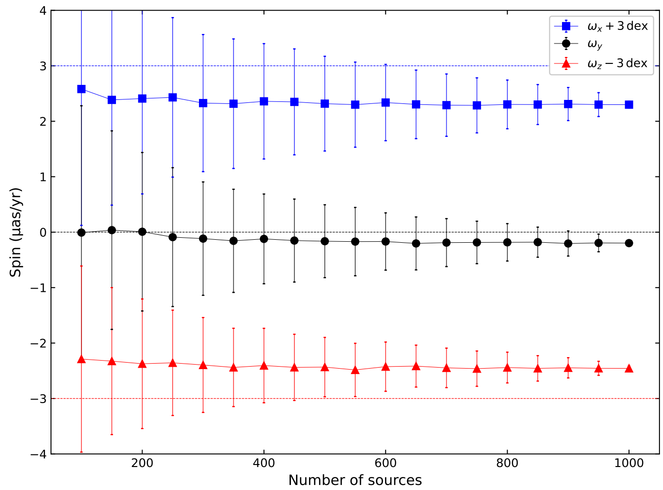

Fig. 2. Global spin estimated from the apparent proper motion versus the sample size used in the bootstrap sampling. The markers and errorbars stand for the mean value and standard deviation from 1000 bootstrap samples, respectively.

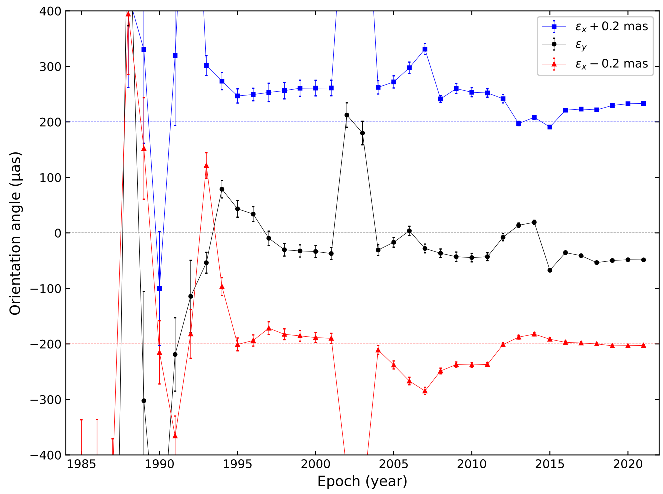

Fig. 3. Orientation of yearly celestial references constructed from the VLBI global solution with respect to the ICRF3 S/X-band catalog based on the ICRF3 defining source subset.

Similarly, the relative orientation angles of the yearly celestial frame based on the coordinate time series become more stable after around 1995 as shown in Fig. 4. The weighted mean value and standard deviation of the orientation angle around the X-, Y-, and Z-axis are $+30 \pm 41\,\mu$as, $-8 \pm 45\,\mu$as, and $-11 \pm 46\,\mu$as, respectively. When only considering the data points after 1995, the corresponding standard deviations were reduced slightly, which ranged from 40 μas to 45 μas.

In short, the axis of the yearly celestial reference frame is stable at the level of 15 − 45 μas.

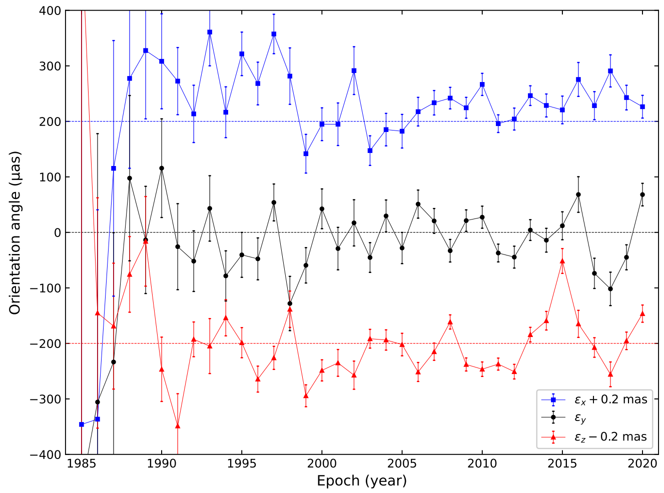

Fig. 4. Orientation of yearly celestial references averaged from the coordinate time series with respect to the ICRF3 S/X-band catalog based on the ICRF3 defining source subset.

Table 2. Relative orientation of various catalogs with referred to the ICRF3 S/X catalogs based on the subset of ICRF3 defining sources.

Catalog	ϵ_x	±	ϵ_y	±	ϵ_z	±
asi2020a	−4	3	+5	2	+5	1
aus2020b	−4	3	+0	3	−9	3
opa2019a	+25	1	−52	1	−1	1
usn2019c	+2	1	+0	1	+12	1
ICRF2	+14	6	+14	6	−4	5
ICRF3 K	−3	11	−15	11	−7	7
ICRF3 X/Ka	−6	20	−11	21	+28	15

Notes. The orientation angle (ϵ_x, ϵ_y, ϵ_z) and the formal uncertainty (±) are estimated by the mean and standard deviation.

4.3. Orientation of various radio catalogs relative to the ICRF3

Table 2 reports the relative orientation of various radio catalogs with referred to the ICRF3 S/X-band catalogs based on the subset of the ICRF3 defining sources. These orientation angles are generally less than 10 μas, except for opa2019a. When comparing the ICRF2 with the ICRF3 S/X-band catalogs, the orientation angle is also on the order of 10 μas. As a result, the difference in the axis direction between celestial reference frames represented by different catalogs at S/X-band is generally within 10 μas.

We compared the relative orientation of representations of the ICRF3 at three bands. The orientation offset is about 10 μas, except for the Y-axis between the K-band and S/X-band, and the Z-axis between the X/Ka-band and S/X-band.

4.4. Orientation agreement among different realizations of ICRS

In order to assess the overall agreement in the axial directions of different realizations of the ICRS, we adopted the bootstrap sampling method as described in Sect. 3.2 and presented the results in Table 3. About two thirds of the whole common sources were picked in each iteration. The ICRF3 S/X catalogs were used as the reference catalog, in which case we assessed the internal alignment precision of the ICRF3. We found that the scatter (standard deviation) of relative orientation of the ICRF2, ICRF3 K-band, and ICRF3 X/Ka-band is all smaller than 7 μas, despite the constant orientation offset. It suggested that the internal alignment precision is on the level of 7 μas or better.

Table 3. Orientation agreement among realizations of the ICRS at different wavelengths.

Catalog	N	ϵ_x	±	ϵ_y	±	ϵ_z	±
wrt. ICRF3 S/X							
ICRF2	2300	+9	3	+14	3	−2	2
ICRF3 K	550	−11	5	−18	4	−7	3
ICRF3 X/Ka	450	−17	7	−2	7	+49	5
wrt. *Gaia* EDR3							
ICRF3 S/X	2100	−2	5	−2	5	−2	5
ICRF3 K	440	−12	14	−12	14	−12	14
ICRF3 X/Ka	384	−8	20	−8	20	−8	20

Notes. The orientation angle (ϵ_x, ϵ_y, ϵ_z) and the formal uncertainty (±) are estimated by the mean and standard deviation.

We also evaluated the potential precision of the VLBI-*Gaia* frame link by setting the *Gaia* EDR3 position as the reference. The agreement in the axis orientation is about 5 μas between the ICRF3 S/X-band and *Gaia* EDR3, 14 μas for the K-band, and 20 μas for the X/Ka-band. Considering that the *Gaia* measurement precision and accuracy will be both continuously improved and so do the VLBI celestial reference frames, these values could be considered as a conservation estimate of the alignment precision that the future radio-to-optical frame link can achieve.

5. Conclusions

1. The stability of the ICRF axes is found to be about 10-45 μas, depending on the methods used.
2. The internal alignment precision of the ICRF3 is on the level of 10-20 μas.
3. The potential precision for the optical-to-radio frame link is no worse than 20 μas and can reach 5 μas for the S/X-band ICRF and the *Gaia*-CRF.

Acknowledgements.

References

Andrei, A. H., Bouquillon, S., de Camargo, J. I. B., et al. 2009, in Journées Systèmes de Référence Spatio-temporels 2008, ed. M. Soffel & N. Capitaine, 199–202
Arias, E. F. & Bouquillon, S. 2004, A&A, 422, 1105
Charlot, P., Jacobs, C. S., Gordon, D., et al. 2020, A&A, 644, A159
Dehant, V., Feissel-Vernier, M., de Viron, O., et al. 2003, Journal of Geophysical Research (Solid Earth), 108, 2275
Feissel-Vernier, M. 2003, A&A, 403, 105
Feissel-Vernier, M., Ma, C., Gontier, A. M., & Barache, C. 2006, A&A, 452, 1107
Fey, A. L., Gordon, D., Jacobs, C. S., et al. 2015, AJ, 150, 58
Fomalont, E., Johnston, K., Fey, A., et al. 2011, AJ, 141, 91
Gaia Collaboration, Mignard, F., Klioner, S. A., et al. 2018, A&A, 616, A14
Gattano, C., Lambert, S. B., & Le Bail, K. 2018, A&A, 618, A80

Lambert, S. 2013, A&A, 553, A122
Lambert, S. 2014, A&A, 570, A108
Lambert, S. B., Dehant, V., & Gontier, A. M. 2008, A&A, 481, 535
Lambert, S. B. & Gontier, A. M. 2009, A&A, 493, 317
Liu, N., Lambert, S. B., Zhu, Z., & Liu, J. C. 2020, A&A, 634, A28
Liu, N., Liu, J. C., & Zhu, Z. 2017, MNRAS, 466, 1567
Ma, C., Arias, E. F., Eubanks, T. M., et al. 1998, AJ, 116, 516
Ma, C., Clark, T. A., Ryan, J. W., et al. 1986, AJ, 92, 1020
MacMillan, D. S., Fey, A., Gipson, J. M., et al. 2019, A&A, 630, A93
Moór, A., Frey, S., Lambert, S. B., Titov, O. A., & Bakos, J. 2011, AJ, 141, 178
Nothnagel, A., Artz, T., Behrend, D., & Malkin, Z. 2017, Journal of Geodesy, 91, 711
Sazhin, M. V., Zharov, V. E., Volynkin, A. V., & Kalinina, T. A. 1998, MNRAS, 300, 287
Schaap, R. G., Shabala, S. S., Ellingsen, S. P., Titov, O. A., & Lovell, J. E. J. 2013, MNRAS, 434, 585
Shabala, S. S., Rogers, J. G., McCallum, J. N., et al. 2014, Journal of Geodesy, 88, 575
Taris, F., Andrei, A., Klotz, A., et al. 2013, A&A, 552, A98
Taris, F., Andrei, A., Roland, J., et al. 2016, A&A, 587, A112
Taris, F., Damljanovic, G., Andrei, A., et al. 2018, A&A, 611, A52
Titov, O., Tesmer, V., & Boehm, J. 2004, in International VLBI Service for Geodesy and Astrometry 2004 General Meeting Proceedings, ed. N. R. Vandenberg & K. D. Baver, 267